arXiv:1403.6826v1 [hep-ph] 26 Mar 2014

Physics Motivation for a Pilot Dark Matter Search at Jefferson Laboratory

Eder Izaguirre, Gordan Krnjaic, Philip Schuster, and Natalia Toro
Perimeter Institute for Theoretical Physics, Waterloo, Ontario, Canada N2L 2Y5
(Dated: March 28, 2014)

It has recently been demonstrated that a program of parasitic electron-beam fixed-target experiments would have powerful discovery potential for dark matter and other new weakly-coupled particles in the MeV–GeV mass range. The first stage of this program can be realized at Jefferson Laboratory using an existing plastic-scintillator detector downstream of the Hall D electron beam dump. This paper studies the physics potential of such an experiment and highlights its unique sensitivity to inelastic "exciting" dark matter and leptophilic dark matter scenarios. The first of these is kinematically inaccessible at traditional direct detection experiments and features potential "smoking gun" low-background signatures.

I. INTRODUCTION

Although overwhelming astrophysical and cosmological evidence supports the existence of dark matter (DM) [1], its identity, interactions, and origin remain elusive. There is currently an active program to probe particle DM scattering with direct detection experiments, annihilation with indirect detection telescopes, and production with particle accelerators [2]. However, most of these efforts are designed to find heavy (10−1000 GeV) DM candidates and sharply lose sensitivity to lighter (sub-GeV) states whose signals are either too feeble or lie in high-background regions. Even direct-detection experiments [3–5] and proposals [6–8] that are expanding sensitivity to GeV-scale DM rely on an elastic scattering channel that is absent or highly suppressed in many DM scenarios [9–16].

Recently it was shown that electron-beam fixed target experiments offer powerful sensitivity to a broad class of dark sector scenarios that feature particles in the elusive MeV-GeV mass range [17, 18]. If DM couples to leptonic currents via mediators of comparable mass, it can be produced copiously in relativistic electron-nucleus collisions and scatter in a downstream detector (see Fig. 1). Electron beam-dump experiments are complementary to dedicated efforts at proton beam facilities [19–23], and have comparable DM scattering yield. Electron-beam experiments can run parasitically on a smaller scale and benefit from negligible beam-related backgrounds.

Jefferson Laboratory (JLab) is currently upgrading its 6 GeV electron beam to operate at 12 GeV energies. The new CEBAF (continuous electron beam accelerator facility) is scheduled to begin delivering $\sim 100\mu$A currents in mid-2014 and presents new opportunities to search for new light weakly coupled particles. A possible first step would be a parasitic pilot experiment using an existing plastic-scintillator detector behind the Hall D electron beam dump, which will receive a ~ 200 nA current [24]. Such an experiment could pave the way for a larger-scale experiment behind a higher-current beam dump [17]. Remarkably, even a small-scale pilot experiment has potential discovery sensitivity to several DM scenarios, which we explore in this paper. A particularly dramatic signal could be seen if DM states are split by $\gtrsim$ MeV, so that DM scattering produces energetic e^+e^- pairs (considered in other contexts in [9, 11, 14, 16, 25–29]).

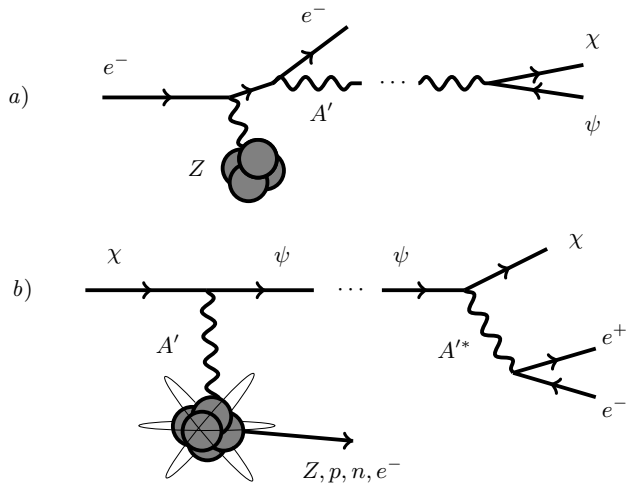

FIG. 1: a) Fermionic DM pair production from A'-sstrahluung in electron-nucleus collisions. In the generic scenario with Dirac and Majorana masses for dark sector fermions, the A' mediator couples off diagonally to the mass eigenstates χ and ψ (see Sec. II B 2). b) Detector scattering via A' exchange inside the detector. If the mass splitting between dark sector states is negligible, both the incoming and outgoing DM states in the scattering process are invisible and can be treated as the same particle. For order one (or larger) mass splittings, χ can upscatter into the excited state ψ, which promptly decays inside the detector via $\psi \to \chi\, e^+e^-$. This process yields a target (nucleus, nucleon, or electron) recoil E_R and two charged tracks, which is a distinctive, low background signature, so nuclear recoil cuts need not be limiting. Processes analogous to both a) and b) can also exist if DM is a scalar – see Sec. II B 1

The basic production and detection processes we consider here parallel those discussed in [17, 19, 20]. Electrons impinging on atomic nuclei in a beam dump can emit light mediator particles that promptly decay to pairs of DM particles or the DM can be radiated via off shell mediator exchange (Figure 1(a)). The pair of DM particles emerge from the beam dump in a highly collimated

beam and pass through the shielding and dirt because their interactions are weak. A fraction of the DM particles scatter off electrons, nucleons, or nuclei via mediator exchange in a downstream detector (Figure 1(b), left). Because the DM particles are relativistic, their scattering can induce multi-MeV recoils of the target which in turn produce scintillation or Čerenkov light.

Our treatment generalizes [17] in three important ways. First, we consider the possibility that the mediator coupling DM to SM matter couples *only* to leptons, not to nucleons — for example, a vector can couple to the conserved $U(1)_{e-\mu}$ current. This scenario produces only electron-scattering, but no associated nucleon/nucleus scattering signal. In this case, DM would not be produced in proton-beam experiments, but neutrino physics does constrain the $U(1)_{e-\mu}$ coupling. Second, whereas [17] focused primarily on quasi-elastic scattering off nucleons, we consider DM-electron, DM-nucleon, and DM-nucleus scattering here. The latter is most significant at low momentum transfers (where it is Z^2-enhanced), but is suppressed by form factors at higher momentum transfers. DM-electron scattering can easily yield multi-GeV electron recoils for the mediator masses of interest, and are therefore particularly visible. Third, and most significantly, we consider a new signal that arises when the DM states have $O(1)$ mass splittings and have appreciable inelastic interactions, as in [9–16]. In this case, the up-scattering of a dark matter state χ into an excited state ψ is followed by a prompt decay $\psi \to \chi e^+ e^-$ (Figure 1(b), right). Thus, the target recoil is accompanied by the GeV-scale energy deposition of the e^+e^- pair, which can carry a significant fraction of the incident beam energy. Because beam-related backgrounds are small and cosmic backgrounds are dominated at much lower energies, the energy deposition from such decays could be a "smoking gun" signal for a light DM candidate even in a small above-ground detector.

The outline of this paper is as follows. Section II presents the simplified models we consider in our analyses and discusses the model dependence of existing constraints. Section III describes the setup of a test run at JLab Hall D (inspired by [30]) and presents our yield projections for different scattering channels. Finally, section V offers some concluding remarks.

II. BENCHMARK SCENARIOS

Viable MeV–GeV-mass dark matter candidates that thermalize in the early Universe require a light mediator through which the DM can annihilate. Surprisingly, there are few *model independent* constraints on light, leptonically coupled mediators in the MeV–GeV mass range (see [23] for a review). Fig. 2 (top) shows the bounds on a vector mediator from precision QED measurements without assuming anything about its decay or scattering signatures. We require only that the mediator couples to leptons with strength ϵe; insertions of virtual A' into diagrams generically correct the lepton-photon vertex and contribute to $(g-2)_{e,\mu}$. A growing program of direct searches for light mediators rely either on visible decays of these mediators [31–54] or their hadronic couplings [19–23]. In this section we consider the constraints on a variety of new mediators and establish benchmark DM scenarios for which electron beam dump experiments are particularly sensitive.

A. Mediators to the Standard Model

We consider two representative possibilities for the mediator interactions with the Standard Model: kinetic mixing with the photon (which couples to all charged leptons and hadrons) and interactions with leptons alone through a $U(1)_{e-\mu}$ coupling. Up to numerical factors, results for the kinetic mixing model can be taken as a proxy for any mediator whose interactions with electrons and light nucleons have comparable strengths. The $U(1)_{e-\mu}$ model is likewise representative of the more general possibility that the mediator interacts with electrons but *not* nucleons.

1. *Kinetically Mixed $U(1)_D$*

For simplicity, it is convenient to frame our discussion in terms a simplified model with a massive, *invisibly decaying* vector boson A' from a broken $U(1)_D$ gauge group. The most general lagrangian for A' contains

$$\mathcal{L} \supset -\frac{1}{4}F'^{\mu\nu}F'_{\mu\nu} + \frac{\epsilon}{2}F^{\mu\nu}F'_{\mu\nu} + \frac{m_V^2}{2}A'_\mu A'^\mu \quad , \qquad (1)$$

where $F'_{\mu\nu} \equiv \partial_{[\mu,}A'_{\nu]}$ is the field strength, $m'_A \sim$ MeV – GeV is the mediator mass, and ϵ is the kinetic mixing, which is naturally in the $10^{-5} - 10^{-2}$ range if generated by loops of heavy particles charged under both dark and visible gauge groups. Diagonalizing the gauge kinetic terms induces an effective coupling to SM currents

$$\mathcal{L} \supset \epsilon A'_\mu \sum_i q_i \overline{f}_i \gamma^\mu f_i \quad , \qquad (2)$$

where f_i is any SM quark or lepton and q_i is its charge. Assuming the A' decays invisibly[1] to pairs of dark-sector states with masses below ~ 68 MeV, this extension faces constraints from BaBar [17, 60], LSND [20], $(g-2)_{e,\mu}$ [55, 61], and rare Kaon decays [57], shown in the bottom panel of Fig. 2.

The interactions in Eq. (2) mediate DM scattering off electrons, coherent scattering off nuclei, quasielastic scattering off nucleons, and inelastic scattering off nuclei.

[1] Constraints on a visibly decaying mediator $A' \to e^+e^-$ are also given in [59], but we do not consider this scenario.

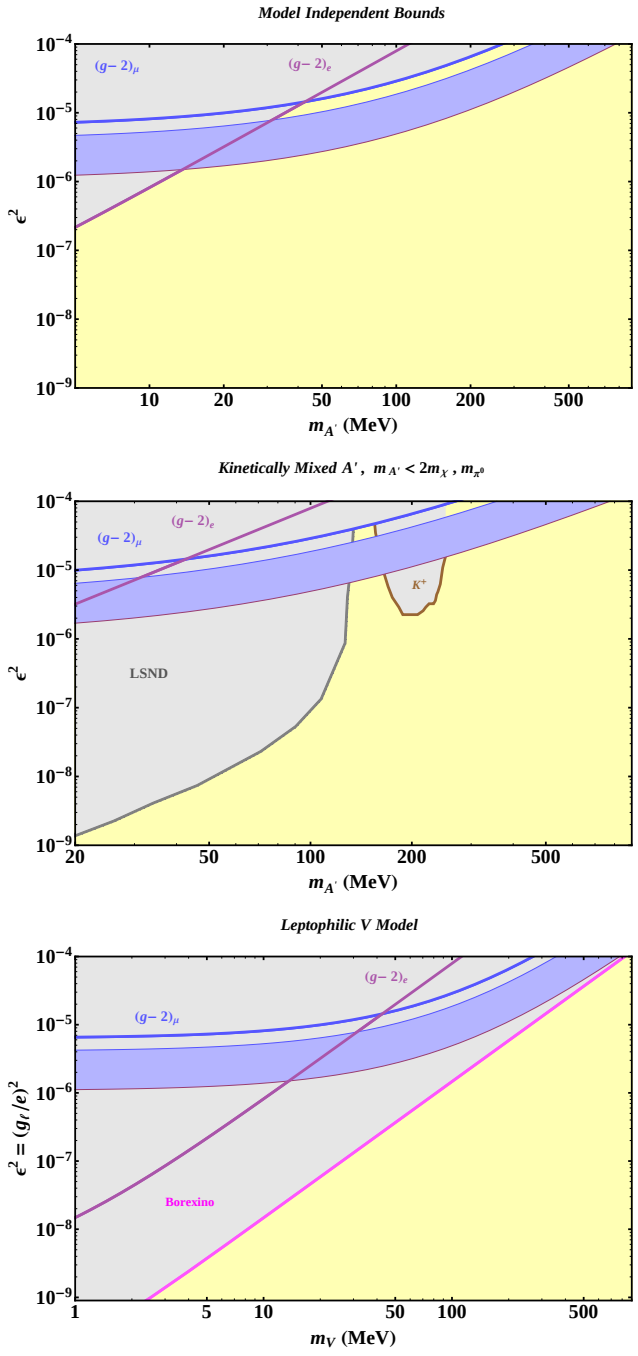

FIG. 2: Top: model independent bounds on an MeV-GeV scae gauge boson that couples only to charged leptons. The purple band is the region that resolves $(g-2)_\mu$ anomaly to within 2σ [55]. Middle: model *dependent* bounds on a kinetically mixed A' from Sec. II A 1 assuming it decays predominantly to two stable, invisible fermions in the dark sector $A' \to \chi\bar{\chi}$ and $m_{A'} \gg 2m_\chi$ as outlined in Sec. II B 2. Additional constraints are from LSND [20], a mono-γ search at BaBar [56], and rare Kaon decays [57]. Bottom: bounds on the leptophilic model from Sec. II A 2. This model requires V couplings to neutrinos which are constrained by Borexino [58].

The last process requires substantial momentum transfer and is not included in our simulations. For a detailed discussion of the signals we simulate in our numerical studies, see Sec. III C and Appendix A.

2. *Leptophilic $U(1)_{e-\mu}$*

The simplest leptonically coupled mediator arises from a $U(1)_{\ell_i-\ell_j}$ gauge extension to the SM [62–67], where $\ell_{i,j} = e, \mu$, or τ and $i \neq j$ are SM leptons. For concreteness, we consider only $U(1)_{e-\mu}$ as the simplest model that allows mediator couplings to electrons. The lagrangian for this mediator contains

$$\mathcal{L} \supset -\frac{1}{4}\mathcal{F}^{\mu\nu}\mathcal{F}_{\mu\nu} + \frac{m_V^2}{2}V_\mu V^\mu + V_\mu \sum_i g_{\ell_i}\bar{\ell}_i\gamma^\mu\ell_i \quad , \quad (3)$$

where $\mathcal{F}_{\mu\nu} = \partial_{[\mu}V_{\nu]}$ is the field strength and g_{ℓ_i} is the $U(1)_{e-\mu}$ charge for lepton ℓ_i.

In this mass range leptophilic invisibly decaying mediators are constrained only by precision QED measurements of $(g-2)_{e,\mu}$ [55, 61] and by neutrino-scattering observations with Borexino [58]. For comparison with the conventional bounds on kinetically mixed gauge bosons, we will present the parameter space in terms of the parameter $\epsilon \equiv g_\ell/e$.

B. Dark Species and Spectra

We now consider simplified models of the dark sector that feature either a complex scalar or Dirac fermion coupled to the SM via one of the mediators in Sec. II A. For simplicity, in this subsection we use the notation appropriate for the $U(1)_D$ model with an A', but the features discussed below apply equally to a $U(1)_{e-\mu}$ gauge boson or any other spin-1 mediator.

A key feature of these models is that the same spontaneous symmetry breaking that gives the mediator a nonzero mass (for concreteness, we consider a perturbative Higgs mechanism) can also split the bosonic/fermionic matter into two real/Majorana states with different masses. The leading mediator coupling in these cases are *generically* off-diagonal. Thus the DM production mode shown in Figure 1(a) always produces one light and one heavy particle, and its scattering (Figure 1(b) left) is always inelastic. The subsequent phenomenology is determined by the excited-state lifetime, which scales as $m_{A'}^4/(\Delta^5\epsilon^2\alpha\alpha_D)$ and so is very sensitive to the size of the splitting. For large enough splittings, the decay occurs inside the detector and the decay products contribute significantly to (or even dominate) the energy deposition from DM scattering (see §II C). These inelastic scenarios are especially important to consider because a thermal origin for dark matter in such models is entirely compatible with constraints on light dark matter derived from measurements of the CMB [68].

1. Scalar Spectra

Consider a complex scalar particle Φ coupled to a $U(1)_D$ gauge boson that gets its mass from the symmetry-breaking vev of a second charged scalar, H_D. If Φ and H_D have equal and opposite charges, the most general Lagrangian contains

$$\mathcal{L} \supset |(\partial_\mu - ig_D A_\mu)\Phi|^2 \; - \; \left(M^2 + \eta|H_D|^2\right)|\Phi|^2 \\ - \; \kappa\Phi^2 H_D^2 - \lambda|\Phi|^4 + h.c., \quad (4)$$

where $g_D = \sqrt{4\pi\alpha_D}$ is the $U(1)_D$ coupling constant to *dark sector* matter. For $\langle H_D\rangle \neq 0$, the potential contains both diagonal and off-diagonal mass terms for Φ, which split the mass-eigenstates. The mass eigenbasis now features two states φ and ϕ whose mass splitting $M_\phi - M_\varphi \equiv \Delta$ is generically of order the common mass scale in the dark sector (or smaller for small κ).

After symmetry breaking, the mass eigenstates couple off-diagonally to the mediator, via the derivative interaction $g_D {A'}_\mu \phi i\partial^\mu \varphi + c.c.$. Thus, in the presence of mass splittings, every A' produced in a beam dump yields a ground state φ and an excited state ϕ, which can generate distinct detector signatures. An incident excited state ϕ scatters by converting into the ground state and inelastically depositing it energy into the target particle via A' exchange. The ground state φ can only interact with the detector by upscattering into the excited state, which for $\Delta < m_{A'}$ decays via $\phi \to A'^* \to \varphi e^+e^-$. In the $\Delta \ll M_\phi$ limit, the width for this process is

$$\Gamma(\phi \to \varphi\, e^+e^-) = \frac{4\epsilon^2\alpha\alpha_D\Delta^5}{15\pi m_{A'}^4} + \mathcal{O}(\Delta^6) \quad , \quad (5)$$

(see Appendix B). For a boost factor of γ, the decay length is

$$\ell_\phi \; = \; \gamma c/\Gamma(\phi \to \varphi\, e^+e^-) \quad (6)$$

$$\simeq 0.01\text{cm}\left(\frac{\gamma}{2}\right)\left(\frac{10^{-3}}{\epsilon}\right)^2\left(\frac{0.1}{\alpha_D}\right)\left(\frac{50\text{ MeV}}{\Delta}\right)^5\left(\frac{m_{A'}}{50\text{ MeV}}\right)^4,$$

so for splittings of order the mediator mass, the decay is microscopic on detector length scales and gives rise to a distinctive signal.

2. Fermionic Spectra

If the A' interacts with a dark sector Dirac fermion $\Psi = (\lambda, \xi^\dagger)$ charged under $U(1)_D$, the Lagrangian in Weyl components is

$$\mathcal{L} \supset i\lambda^\dagger\bar\sigma^\mu D_\mu\lambda + i\xi^\dagger\bar\sigma^\mu D_\mu\xi + m(\xi\lambda + \xi^\dagger\lambda^\dagger) + h.c. \quad (7)$$

Again, for appropriate charge assignments, there are also Yukawa interactions

$$\mathcal{L} \supset y_\lambda H_D\lambda\lambda + y_\xi H_D^\dagger\xi\xi + h.c., \quad (8)$$

which induce Majorana mass terms after spontaneous symmetry breaking. Diagonalizing the fermion masses yields states ψ and χ with masses $\sim m \pm y\langle H_D\rangle$, respectively and the gauge mediator couples off diagonally to the mass eigenstates via the $g_D {A'}_\mu \psi^\dagger\bar\sigma^\mu\chi + h.c.$ interaction.

Scattering through A' exchange is now necessarily inelastic and the heavier state ψ can now de-excite (see Appendix B) with width

$$\Gamma(\psi \to \chi\; e^+e^-) = \frac{8\epsilon^2\alpha\alpha_D\Delta^5}{15\pi m_{A'}^4} + \mathcal{O}(\Delta^6), \quad (9)$$

which is parametrically comparable to the corresponding scalar result in Eq. (5).

C. Smoking Gun Signals

In [17] it was shown that electron beam dumps have sensitivity to quasi-elastic DM-nucleon scattering, $\chi n \to \chi n$, via A' exchange, however, for continuous wave (CW) beams [2], exploiting this process typically requires shielding or vetoing environmental backgrounds. However, there are two *smoking gun* signals with such high energy deposition that the backgrounds can be dramatically reduced or even eliminated (see §III B); even a $\sim$ 10-event signal of these types could suffice for a convincing discovery.

1. High Energy Electron Recoils

For both mediator models in Sec. II A and both dark sector scenarios in Sec. II B, a typical DM particle produced in the beam dump can scatter off detector electrons and produce visible recoil energies. The dominant backgrounds for this channel comes from cosmic muons which either decay in flight or are stopped in the detector and decay at rest. Sec. III B will give estimates for these backgrounds and we comment on their reducibility.

2. Inelastic DM Transitions

Models with non-minimal dark scalar (or fermion) spectra offer a unique signature to be exploited at an electron beam-dump experiment. If excited states ϕ or

[2] For a CW beam, the beam-on live-time coincides with the total duration of the experiment, which is on the order of several-months, so timing is difficult and the detector encounters the maximum flux of environmental backgrounds over that time interval. In contrast, a *pulsed* beam delivers electrons in small, concentrated bunches, so the beam-on time is typically $\ll 10^{-2}$ of the total experimental run, which dramatically reduces the detector's effective exposure to environmental backgrounds.

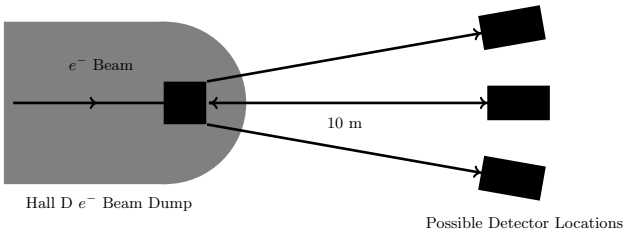

FIG. 3: Overhead view of the proposed experimental configuration behind Hall D. The detector can be placed either on-axis or displaced off-axis to take advantage of better acceptances for certain classes of DM particles.

ψ decay promptly on scales $\lesssim 10$ cm, then a unique handle on DM comes from the ground-states upscattering via the off-diagonal gauge interactions in Sec. II B and transitioning into the short-lived excited states

$$\chi T \to \psi T \to (\psi \to \chi\ e^+e^-)T \tag{10}$$

for fermions χ, ψ. Similarly for scalars we have

$$\varphi T \to \phi T \to (\phi \to \varphi\ e^+e^-)T, \tag{11}$$

where T can be a target nucleus, nucleon, or electron. The detector signature of this process is a target recoil accompanied by an energetic e^+ e^- pair. This final state is difficult to mimic by a beam-originated or cosmic-originated background event.

III. TEST RUN SETUP

In the test-run set up discussed in this paper, we assume placement of a small detector above ground roughly 10 m behind the electron beam-dump at JLab Hall D. Fig. 3 shows a schematic of possible test-run setups. In a year of normal operations, Hall D will receive currents $\sim$ 200 nA from CEBAF for a few months, which this experiment can use parasitically. We therefore consider a benchmark of 10^{19} electrons on target (EOT) over a beam-on live time of 90 days. The possibility of an off-axis detector is considered because the beamline into the dump is slightly below ground level. An above-ground experiment would therefore be slightly misaligned with the beam axis.

A. Detector

Inspired by the existing CORMORINO prototype [30], we simulate DM-SM scattering in a 40 cm $\times$ 30 cm $\times$ 30 cm detector of NE110 polyvinyltoluene ($C_{27}H_{30}$) plastic-scintillator. Fig. 4 shows the angular distribution with respect to the beam-line for various mediator masses for both fermion and scalar DM.

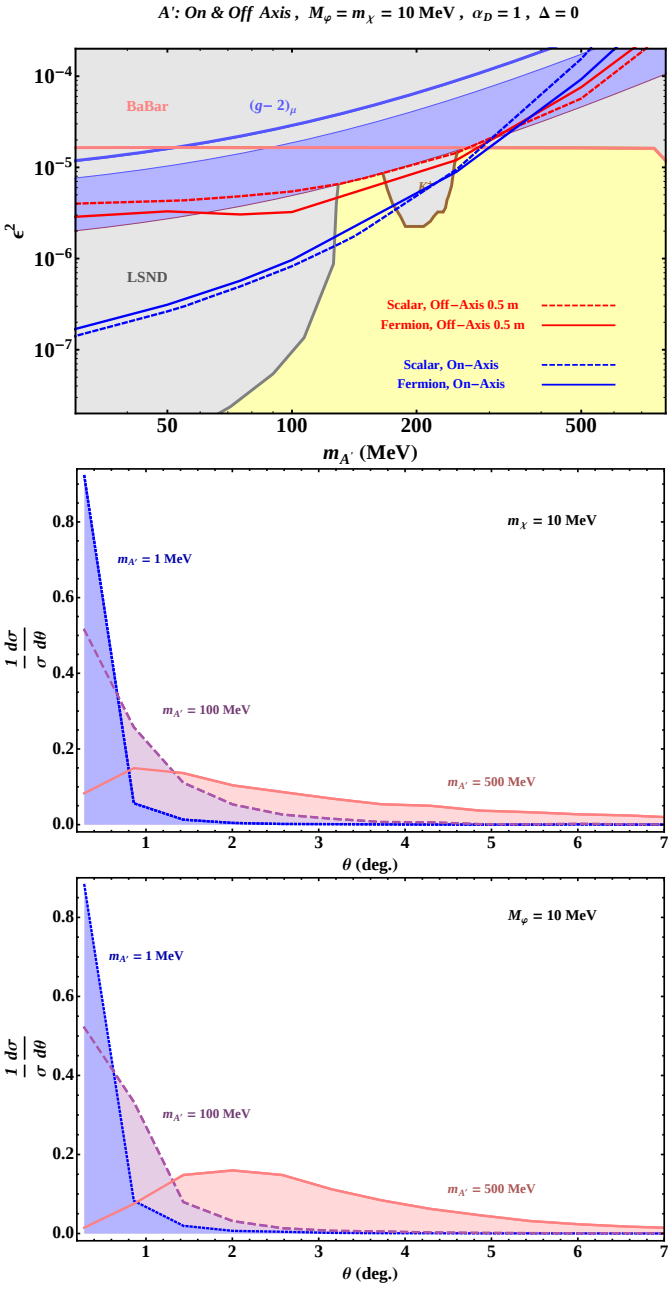

FIG. 4: Top: yield comparison for scalar and fermion DM using both on and off-axis detector positions (see Fig. 3). Middle and bottom: angular distributions for 10 MeV fermion and scalar production respectively. Note the off-axis peak near $\theta \sim 2^o$, in the scalar distribution for $m_{A'} = 500$ MeV.

B. Backgrounds

The 12 GeV CEBAF at Jefferson Laboratory delivers electrons to experimental Halls A, B, C, and D. The proposed test-run in this article assumes that such an experiment would take place downstream of Hall D and follow the layout in Fig. 3. Given the geography surrounding Hall D, a detector placed 10 meters behind the

beam dump would be near or at ground level (the latter if run in off-axis mode). The various backgrounds associated with the test-run can be divided into two kinds: those originating from the beam, and those unrelated to the beam (cosmic-originated events). Beam-related backgrounds were estimated to be negligible even with 10^{22} EOT [17], so we ignore these for the remainder of this section. In what follows we estimate the beam-unrelated backgrounds for leptophilic (electron channel) and inelastic models.

Models where up-scattering to an excited state is followed by a prompt decay of the excited state leave a unique signature. The signal consists of an e^+e^- pair, collectively depositing $\sim$ GeV energy, and a hard recoil from either an electron, nucleon, or nucleus. If each of these particles could be separately resolved, then this signal would be easily separated from cosmogenic backgrounds. For example, if the excited state lifetime is cm-scale, then the recoil and e^+e^- pair would frequently appear in different cells of the detector. Even for prompt decays and a simple plastic scintillator detector — where the total energy deposited is probably the only observable signal — this energy may be sufficient to stand out over backgrounds. The same is true of the electron-scattering signal.

The most important background process comes from cosmic muons which then decay to an electron. There are two possibilities to consider: stopped and decay-in-flight muons. The former can be removed entirely by vetoing on muon hits in a window as large as 100 μs and by cutting on $E_R > m_\mu \approx 52.5$ MeV. The timing window can be applied while still having little effect ($\sim 1\%$) on the detector livetime.

The rate of muon decays in flight within the detector can be inferred from measurements of the muon flux at sea-level [69]. For a CORMORINO-sized detector, we estimate a total rate of $\approx 10^{-2}$ Hz. In 90 days of beam-on live time, this gives approximately 10^5 decay-in-flight muons. While this background component is quite sizeable, it is also reducible with a high efficiency by vetoing events with electronic activity coincident with an incoming charged particle. Furthermore, most of the decaying muons are significantly less energetic than the the multi-GeV signals from electron recoils or de-excitation. For example, requiring $E_\mu > 2$ GeV reduces the decay-in-flight rate to $\approx 6 \times 10^{-4}$ Hz. Assuming a 10^3 background-rejection efficiency yields $\mathcal{O}(10)$ decay-in-flight muon events in 90 days. In contrast, demanding requiring $E_R > 2$ GeV has a weak (negligible) effect on the electron-recoil (inelastic de-excitation) signal efficiencies (See Fig. 5).

In Sec III C we discuss the details of the signal simulation. In Sec. IV we give sensitivity estimates for the two classes of signals studied so far. These assume sensitivity at the 10-event level based on this estimates given above. Though we do not explicitly model energy thresholds or beam degradation, these are expected to be at most $O(1)$ corrections to the signal yield.

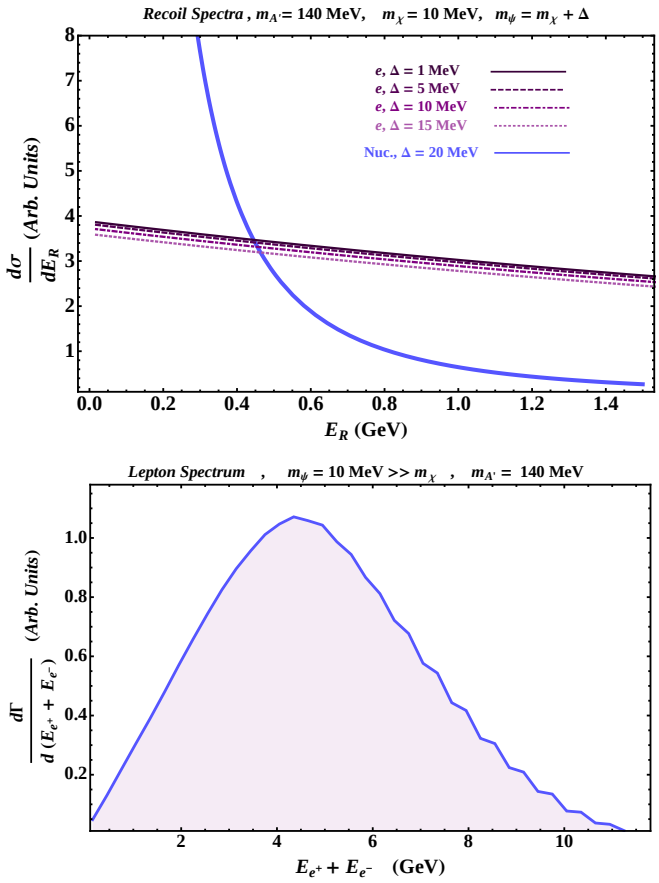
Recoil Spectra , $m_{A'}$ = 140 MeV, m_χ = 10 MeV, $m_\psi = m_\chi + \Delta$
e, Δ = 1 MeV
e, Δ = 5 MeV
e, Δ = 10 MeV
e, Δ = 15 MeV
Nuc., Δ = 20 MeV
$\frac{d\sigma}{dE_R}$ (Arb. Units)
E_R (GeV)
Lepton Spectrum , m_ψ = 10 MeV >> m_χ , $m_{A'}$ = 140 MeV
$\frac{d\Gamma}{d(E_{e^+} + E_{e^-})}$ (Arb. Units)
$E_{e^+} + E_{e^-}$ (GeV)

FIG. 5: Top: Differential recoil spectra in arbitrary units for fermion DM scattering inelastically off electrons with different mass splittings Δ and a thick blue curve (color online) denoting the nucleon recoil distribution, whose shape does not change visually for the parameters we consider in this paper. Each differential cross section is convolved with a monte carlo distribution of incoming χ energies that pass through the detector. Bottom: Lab frame distribution of the combined electron and positron energies after $\psi \to \chi e^+ e^-$ de-excitation for various ψ energies in the $m_\psi \gg m_\chi$ limit. Note that beam degradation (not simulated) would broaden the distribution and pull it towards lower energies. Moreover, for $\Delta \lesssim m_\chi$ the peak energy scales as $\frac{E_{\rm beam}}{2}\frac{\Delta}{m_\psi}$.

C. Simulation

The calculation of the signal yield is factorized into two reactions which are analogous to QED processes: production and re-scattering. On the production side, we use a modified version of `Madgraph 4` to simulate the process depicted in the top panel of Fig. 1

$$eZ \to (A'^{(*)} \to \chi\bar{\chi})eZ, \tag{12}$$

where Z stands for an individual nucleus in the beam dump target, made mostly of aluminum. A nuclear form factor from [70] was used in the modified `Madgraph` version. The production simulation is used to extract the

dN/dE, the energy profile for DM particles that pass through the detector. We do not model the effects of beam degeneration as it passes through the dump on dN/dE, but instead model only the production in the first radiation length of the dump. The resulting signal yield is given by

$$Y = n_T \ell_D \int_{E_c}^{\infty} dE_R \int_{E_m(E_R)}^{\infty} dE \, \frac{dN}{dE} \frac{d\sigma}{dE_R} \quad , \qquad (13)$$

for each scattering channel. Here n_T is the target particle density, ℓ_D is the longitudinal detector length, E_c is the experimental cut on target recoils, E is the incoming DM energy, $E_m(E_R)$ is the minimum energy for an incident particle to induce a target recoil energy E_R, and $d\sigma/dE_R$ is the differential cross section for a given channel – see Appendix A.

The detector reactions considered in this article are depicted schematically in Fig. 1 (bottom) for fermionic DM; analogous processes apply in the scalar scenario. Following the notation of sections II B 2 and II B 1, for the fermionic and scalar DM scenarios, the signatures of interest are

$$\chi\, T \;\to\; (\psi \to \chi\, e^+e^-)\, T \quad , \qquad (14)$$
$$\varphi\, T \;\to\; (\phi \to \varphi\, e^+e^-)\, T \quad , \qquad (15)$$

where T is a target nucleus (coherent scattering), nucleon (quasi-elastic scattering), or electron. In Fig. 5 (top) we show the electron and nucleon recoil distributions for different values of Δ using a monte carlo distribution of incoming DM energies that pass through the detector and (bottom) the lab frame e^+e^- energy distribution for different energies of the excited state.

Unless otherwise specified, the recoil energy thresholds used in the analysis are 100 MeV for incoherent and electron scattering, and 100 keV for coherent nuclear scattering. For nuclear coherent scattering, a lower threshold is used to enhance the signal and get the Z^2 enhancement. In addition to a neutral current coherent scatter, one or more of the electrons from the decay of the excited state are required to scatter in the detector. This signature - an electron signal and a coherent scatter - renders a search for these classes of signals background-free.

IV. RESULTS

The test-run set-up discussed in this paper can have discovery potential for new dark matter scenarios. In what follows, we discuss the sensitivity levels to the two smoking gun signals discussed in Sec. II C.

A. Leptophilic scenario potential

One kind of new physics that a test-run at JLab can be sensitive to is that of a leptophilic mediator between DM and the SM. Fig. 6 shows the 10-event signal yields for electron scattering in the context of a leptophilic A'. The coupling between the DM and the A' is given by g_D and is assumed to be 1 for this scenario. Existing constraints, particularly those coming from solar neutrinos experiments already set strong bounds on the parameter space of this scenario. However, a full-scale experiment as discussed in [17] can cover significant new ground.

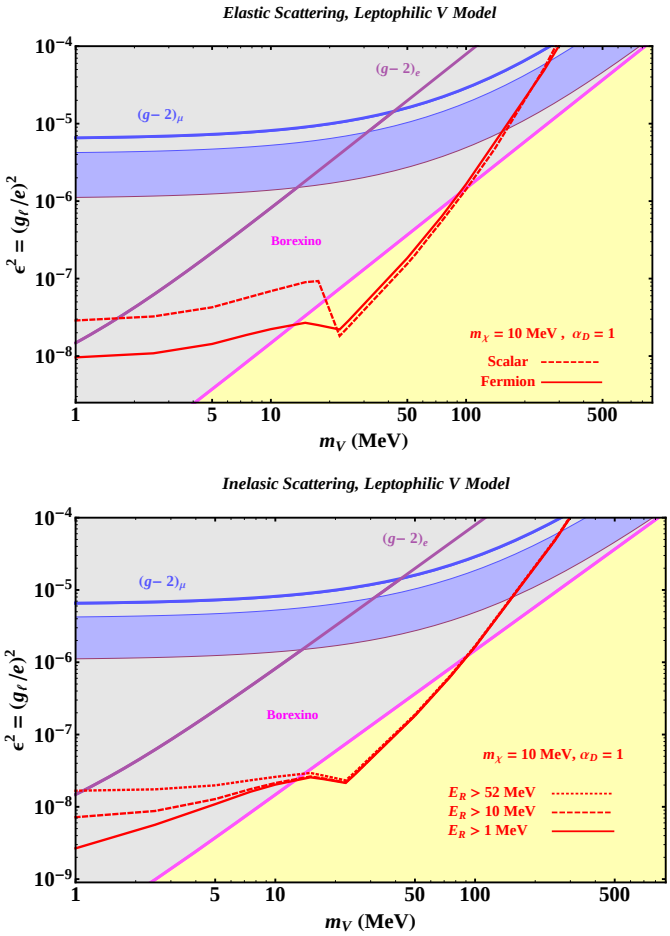

FIG. 6: Top: solid and dashed red curves (color online) show 10 event contours for fermionic and scalar DM respectively scattering off detector electrons via leptophilic V boson exchange (see Sec. II A 2 and II B). The Borexino constraint is extracted from [58]. Bottom: The 10-event sensitivity for different electron recoil energy thresholds.

B. Inelastic transitions potential

A small test run has particularly dramatic sensitivity to non-minimal dark sectors, where a DM excited state can decay in the detector, depositing over a GeV of energy. Both the ground (χ or φ for fermion and scalar DM, respectively) and the excited states (ψ and ϕ) are produced in the beam-dump through an A' radiated by an

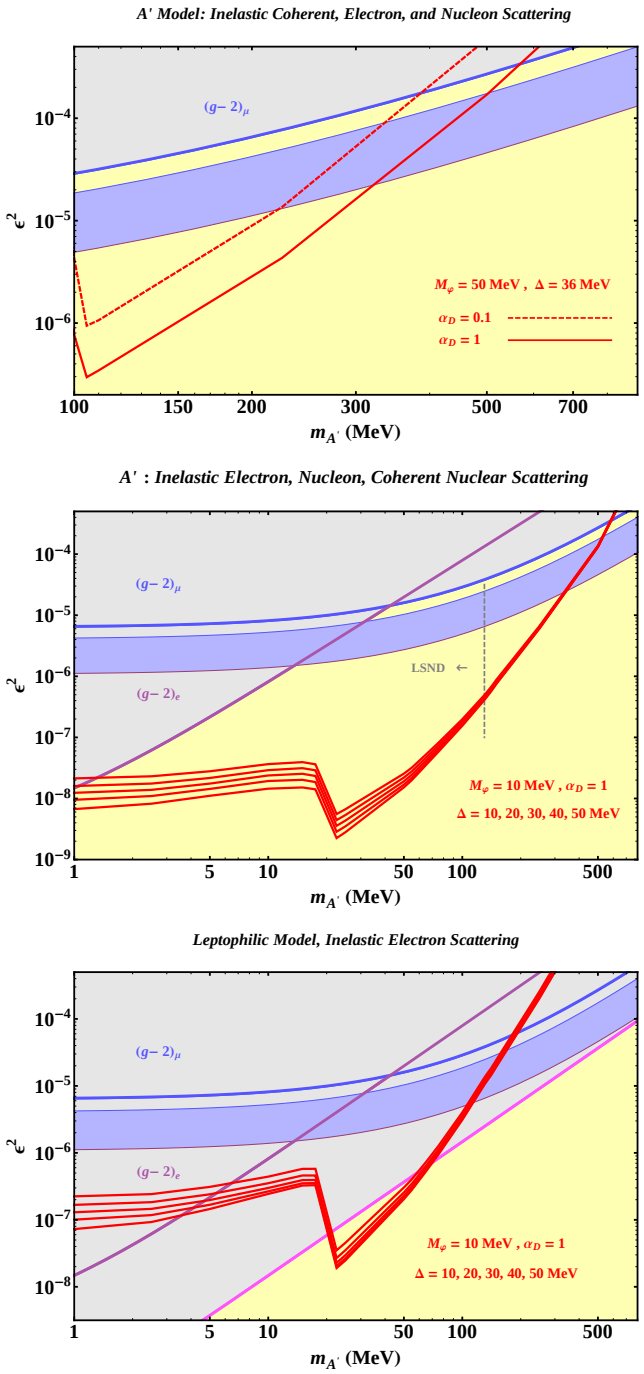

FIG. 7: Scalar upscattering assuming $\phi \to \varphi + e^+e^-$ de-excitation in the A' (top, middle) and leptophilic (bottom) scenarios. Top: α_D overlay for $M_\varphi + M_\phi = m_{\pi^0}$, which is inaccessible at LSND. Middle: A' mediated inelastic upscattering for various mass splittings. In this parameter space, there is a potential constraint from LSND [20] since electrons from the de-excitation can mimic target-electron recoils inside the detector, but a full analysis is beyond the scope of this work. The de-excitation signal is vetoed by the BaBar and rare K^+ decay searches shown in the middle plot of Fig. 2.

electron. For prompt excited states de-excitations, only the ground state makes it to the detector downstream of the beam dump, where it can up-scatter to the excited state. The latter then de-excites within the detector for certain regions of the parameter space. The top and middle plots in Fig. 7 show the 10-event level sensitivity at a test-run for the scalar DM scenario, for fixed choices of $\Delta = M_\phi - M_\varphi$. The Δ is chosen so as to have a prompt de-excitation within the detector. Thus, at least one of the e^+ e^- pair is visible, regardless of whether the ground state φ up-scatters off of a nucleus, nucleon, or electron in the detector, and regardless of the recoil energy. Note that B-factory and rare Kaon decay searches are insensitive to this scenario, because these analyses veto on extra event activity. Constraints from LSND for $m'_A < m_{\pi^0}$ do apply to this scenario, but are difficult to model; we simply indicate the kinematic limit to LSND sensitivity in Fig. 7(middle). Fig. 7 (bottom) shows similar projections varying Δ in the leptophilic scenario.

V. CONCLUSION

In this paper we have shown that a test run for a parasitic fixed-target experiment to search for DM at Jefferson Laboratory could have sensitivity to several well motivated scenarios in only a few months of livetime. Motivated by efforts to launch such a test run experiment [24], we considered signal yields for a small (sub meter-scale) plastic scintillator detector positioned above ground 10 meters downstream of a fixed target – a geometry similar to that at the existing Hall D beam dump. With 10^{19} electrons on target, signal yields are sufficiently high to give a test run experiment unprecedented sensitivity to DM that couples to the visible sector through leptophilic mediators. The same experiment can also probe scenarios where the DM upscatters into an excited state. In this case, the excited state's decay into e^+e^- deposits GeV-scale energy in the detector, irrespective of the target electron, nucleus, or nucleon's recoil energy. These signals can deposit considerably higher energies than the dominant cosmogenic backgrounds. These findings suggest that a small test-run demonstrating the viability of electron beam dump searches for light dark matter will provide new sensitivity to unexplored dark matter scenarios.

Acknowledgments

We thank Brian Batell, Rouven Essig, John Jaros, Maxim Pospelov, Brian Shuve, and especially Haipeng An, Marco Battaglieri, Elton Smith, Stepan Stepanyan, and Raffaella De Vita for helpful conversations. The Perimeter Institute for Theoretical Physics is is supported by the Government of Canada through Industry Canada and by the Province of Ontario.

Appendix A: Detector Scattering

Scalar Amplitude

The amplitude for scattering $\varphi_1(p_1) + T(p_2) \to \varphi_2(k_1) + T(k_2)$ through a kinetically mixed photon is

$$\mathcal{A} = \frac{\epsilon e g_D}{(t - m_{A'}^2)} \bar{u}(k_2)(\not{p}_1 + \not{k}_1)u(p_2) \tag{A.1}$$

where $t \equiv (p_2 - k_2)^2$ is the usual Mandelstam variable and φ_i carries mass m_i. Squaring and averaging (summing) initial (final) state spins

$$\begin{aligned}|\overline{\mathcal{A}}|^2 \;=\; & \frac{2(\epsilon e g_D)^2}{(t - m_{A'}^2)^2}\Big\{(k_2\cdot p_1)(p_2\cdot p_1) + (k_2\cdot p_1)(p_2\cdot p_1) \\ & -(k_2\cdot p_2)(p_1\cdot p_1) + (k_2\cdot p_1)(p_2\cdot k_1) + (k_2\cdot k_1)(p_2\cdot p_1) \\ & -(k_2\cdot p_2)(p_1\cdot k_1) + (k_2\cdot k_1)(p_2\cdot k_1) + (k_2\cdot k_1)(p_2\cdot k_1) \\ & -(k_2\cdot p_2)(k_1\cdot k_1) + (k_2\cdot k_1)(p_2\cdot p_1) + (k_2\cdot p_1)(p_2\cdot k_1) \\ & -(k_2\cdot p_2)(k_1\cdot p_1) + m_T^2\left[m_1^2 + m_2^2 + 2(p_1\cdot k_1)\right]\Big\}. \end{aligned} \tag{A.2}$$

Fermionic Amplitude

The generic matrix element for fermion scattering $\chi_1(p_1) + T(p_2) \to \psi(k_1) + T(k_2)$ is

$$\mathcal{A} = \frac{\epsilon e g_D}{(t - m_{A'}^2)}[\bar{u}(k_2)\gamma^\mu u(p_2)][\bar{u}(k_1)\gamma^\mu u(p_1)] \tag{A.3}$$

where χ_i carries mass m_i. Squaring and averaging initial state spins

$$\begin{aligned}|\overline{\mathcal{A}}|^2 \;=\; & \frac{8(\epsilon e g_D)^2}{(t - m_{A'}^2)^2}\Big[(k_1\cdot k_2)(p_1\cdot p_2) + (k_2\cdot p_1)(p_2\cdot k_1) \\ & -m_1 m_2(k_2\cdot p_2) - m_T^2(p_1\cdot k_1) + 2m_1 m_2 m_T^2\Big] \end{aligned} \tag{A.4}$$

Cross Section

The differential cross section in the CM frame is

$$\frac{d\sigma}{d\Omega^*} \;=\; \frac{|\overline{\mathcal{A}}|^2}{64\pi^2 s}\frac{|\vec{k}^*|}{|\vec{p}^*|} \tag{A.5}$$

In terms of the lab frame recoil energy, the angular measure is $d\cos\theta^* = (m_n/|\vec{p}^*||\vec{k}^*|)dE_R$, where the quantities

$$|\vec{k}^*|^2 \;=\; \frac{(s - m_T^2 - m_2^2)^2 - 4m_T^2 m_2^2}{4s} \tag{A.6}$$

$$|\vec{p}^*|^2 \;=\; \frac{(s - m_T^2 - m_1^2)^2 - 4m_T^2 m_1^2}{4s} \tag{A.7}$$

are the CM frame momenta for each particle in the initial and final state, respectively.

If the target is a detector nucleus, there is additional form factor suppression, so we modify the differential cross section with the replacement

$$\frac{d\sigma}{dE_R} \longrightarrow F(E_R)\frac{d\sigma}{dE_R} \quad , \tag{A.8}$$

where, for momentum transfer $q \equiv \sqrt{2m_N E_R}$, the Helm form factor is [71, 72]

$$F(E_R) = \left(\frac{3j_1(qr)}{qr}\right)^2 e^{-s^2q^2} \quad , \tag{A.9}$$

$$r = \left(c^2 + \frac{7}{3}\pi^2 a^2 - 5s^2\right)^{1/2} \quad , \tag{A.10}$$

where $c = (1.23A^{2/3} - 0.6)$ fm, $s = 0.9$ fm and $a = 0.52$ fm.

Total Event Rate

For each target species T in the detector (e.g. electrons, nucleons, or nuclei), the total event rate is formally

$$Y = n_T \ell_D \int_{E_{R,c}}^{\infty} dE_R \int_{E_m(E_R)}^{\infty} dE\, \frac{dN}{dE}\frac{d\sigma}{dE_R} \quad , \tag{A.11}$$

where ℓ_D is a characteristic detector length scale, $E_{R,c}$ is the experimental cut on recoil energies; inelastic kinematics require there to be a minimum recoil energy for a given splitting regardless of the cut, but this is typically far below any feasible experimental cut. The minimum incoming energy required for an incident particle of mass m_1 to scatter into a state of mass m_2 for a fixed recoil energy E_R

$$E_m \;=\; \frac{(E_R - m_T)\left[m_2^2 - m_1^2 + 2m_T(E_R - m_T)\right] + \sqrt{\mathcal{G}}}{4m_T(E_R - m_T)} \quad , \tag{A.12}$$

where we define

$$\begin{aligned}\mathcal{G} \equiv (E_R - m_T)(E_R + m_T)\Big\{&\left[(m_1 - m_2)^2 + 2m_T(E_R - m_T)\right] \\ &\times\left[(m_1 + m_2)^2 + 2m_T(E_R - m_T)\right]\Big\}, \end{aligned} \tag{A.13}$$

and the energy profile dN/dE is normalized to the number of DM particles passing through the detector.

Appendix B: Three Body Decays

In this appendix we generalize the results from [73] and compute the de-excitation decays in the inelastic scenario where a DM particle up scatters into a heavier dark-sector state and promptly de-excites to a three-body final state inside the detector.

Fermion Decay

For fermions, the amplitude for de-excitation via $\psi(\ell_i) \to \chi(\ell_f)\ e^+(p_+)e^-(p_-)$ is

$$\mathcal{M}_\psi = \epsilon e g_D \frac{[\bar{u}(p_2)\gamma^\mu u(p_1)][\bar{u}(p_+)\gamma_\mu v(p_-)]}{2(p_+\cdot p_-) - m_{A'}^2} \quad , \quad \text{(B.1)}$$

Squaring and summing spins, we have

$$|\overline{\mathcal{M}}_\psi|^2 = \frac{16\,(\epsilon e g_D)^2}{[m_{A'}^2 - 2(p_+\cdot p_-)]^2}\Big[(p_+\cdot p_2)(p_-\cdot \ell_i) + (p_+\cdot \ell_i)(p_-\cdot \ell_f) - m_2 m_1 (p_+\cdot p_-)\Big] \quad \text{(B.2)}$$

Scalar Decay

For scalar decays, the three-body amplitude for $\phi(\ell_i) \to \varphi(\ell_f)\ e^+(p_+)e^-(p_-)$ is

$$\mathcal{M}_\phi = \frac{\epsilon e g_D\, \bar{u}(p_+)(\not{\ell}_i + \not{\ell}_f)v(p_-)}{2(p_+\cdot p_-) - m_{A'}^2} \quad , \quad \simeq \frac{2\epsilon e g_D\, \bar{u}(p_+)\not{\ell}_f v(p_-)}{2(p_+\cdot p_-) - m_{A'}^2} \quad . \quad \text{(B.3)}$$

Squaring and summing leptons spins yields

$$|\overline{\mathcal{M}}_\phi|^2 = \frac{16\,(\epsilon e g_D)^2\big[2(p_+\cdot \ell_f)(p_-\cdot \ell_f) - m_1^2(p_+\cdot p_-)\big]}{(m_{A'}^2 - 2p_+\cdot p_-)^2} \quad , \quad \text{(B.4)}$$

Total Width

The width for both cases can be written

$$\Gamma(\phi/\psi) = \frac{1}{(2\pi)^3(8m_{\phi/\psi})}\int_0^\Delta dE_+ \int_{E_+-\varepsilon}^{\varepsilon} dE_- |\overline{\mathcal{A}}_{\phi/\psi}|^2 \quad , \text{(B.5)}$$

where the parameter

$$\varepsilon \equiv \frac{\Delta - E_+}{1 - 2E_+/m_{\phi/\psi}} \quad , \quad \text{(B.6)}$$

is the maximum energy of the final state e^- for a fixed E_+. Using the kinematic identities in the limit $\Delta \ll m_{\psi,\phi}$

$$p_+\cdot p_- = m_{\phi/\psi}(E_+ + E_- - \Delta) \quad \text{(B.7)}$$
$$\ell_f\cdot p_\pm = m_{\phi/\psi}(\Delta - E_\mp) \quad \text{(B.8)}$$
$$\ell_i\cdot p_\pm = m_{\phi/\psi}E_\pm \quad \text{(B.9)}$$

we obtain

$$\Gamma(\phi \to \varphi\ e^+e^-) = \frac{4\epsilon^2\alpha\alpha_D\Delta^5}{15\pi m_{A'}^4} + \mathcal{O}(\Delta^6)\ , \quad \text{(B.10)}$$

$$\Gamma(\psi \to \chi\ e^+e^-) = \frac{8\epsilon^2\alpha\alpha_D\Delta^5}{15\pi m_{A'}^4} + \mathcal{O}(\Delta^6)\ , \quad \text{(B.11)}$$

which confirm Eqs. (5) and (9).

Decay-Signal Yield

In addition to the target recoil yield, If the coupling to the A' is off-diagonal between different mass eigenstates, there is a signal from the decay of the excited state inside the detector. Following the conventions in Eq. (A.11), the yield of de-excitation events is

$$Y = n_T \ell_D \int_{E_{R,c}}^\infty dE_R \int_{E_m(E_R)}^\infty dE\, \xi(E,E_R)\frac{dN}{dE}\frac{d\sigma}{dE_R}\ , \quad \text{(B.12)}$$

where $\xi \equiv \mathcal{P}\mathcal{F}$ is an efficiency factor for which

$$\mathcal{P}(E,E_R) = 1 - e^{-\ell_D/\ell_{\phi,\psi}} \quad , \quad \text{(B.13)}$$

is the decay probability inside the detector, $\ell_{\phi,\psi} \equiv c\gamma/\Gamma_{\phi,\psi}$ is the decay length, and γ is the decaying particle's boost factor in the lab frame. The function

$$\mathcal{F}(E,E_R) \equiv \frac{1}{\Gamma_{\phi,\psi}}\int_{E_{\rm cut}^\pm}^{\gamma\Delta} dE_\pm \frac{d\Gamma_{\phi,\psi}}{dE_\pm} \quad \text{(B.14)}$$

ensures that only the visible fraction of decay byproduct is counted.

[1] L. Bergstrom, Annalen Phys. **524**, 479 (2012), 1205.4882.
[2] J. Beringer et al. (Particle Data Group), Phys.Rev. **D86**, 010001 (2012).
[3] R. Agnese et al. (SuperCDMSSoudan Collaboration), Phys.Rev.Lett. **112**, 041302 (2014), 1309.3259.
[4] J. Barreto et al. (DAMIC Collaboration), Phys.Lett. **B711**, 264 (2012), 1105.5191.
[5] R. Essig, A. Manalaysay, J. Mardon, P. Sorensen, and T. Volansky, Phys.Rev.Lett. **109**, 021301 (2012), 1206.2644.
[6] R. Essig, J. Mardon, and T. Volansky, Phys.Rev. **D85**, 076007 (2012), 1108.5383.
[7] P. W. Graham, D. E. Kaplan, S. Rajendran, and M. T. Walters, Phys.Dark Univ. **1**, 32 (2012), 1203.2531.
[8] G. Gerbier, I. Giomataris, P. Magnier, A. Dastgheibi, M. Gros, et al. (2014), 1401.7902.
[9] D. P. Finkbeiner and N. Weiner (2014), 1402.6671.
[10] D. Tucker-Smith and N. Weiner, Phys.Rev. **D64**, 043502 (2001), hep-ph/0101138.
[11] D. P. Finkbeiner and N. Weiner, Phys.Rev. **D76**, 083519

(2007), astro-ph/0702587.
[12] S. Chang, G. D. Kribs, D. Tucker-Smith, and N. Weiner, Phys.Rev. **D79**, 043513 (2009), 0807.2250.
[13] Y. Cui, D. E. Morrissey, D. Poland, and L. Randall, JHEP **0905**, 076 (2009), 0901.0557.
[14] D. P. Finkbeiner, T. R. Slatyer, N. Weiner, and I. Yavin, JCAP **0909**, 037 (2009), 0903.1037.
[15] S. Chang, N. Weiner, and I. Yavin, Phys.Rev. **D82**, 125011 (2010), 1007.4200.
[16] M. Pospelov, N. Weiner, and I. Yavin (2013), 1312.1363.
[17] E. Izaguirre, G. Krnjaic, P. Schuster, and N. Toro (2013), 1307.6554.
[18] M. D. Diamond and P. Schuster, Phys.Rev.Lett. **111**, 221803 (2013), 1307.6861.
[19] B. Batell, M. Pospelov, and A. Ritz, Phys.Rev. **D80**, 095024 (2009), 0906.5614.
[20] P. deNiverville, M. Pospelov, and A. Ritz, Phys.Rev. **D84**, 075020 (2011), 1107.4580.
[21] P. deNiverville, D. McKeen, and A. Ritz, Phys.Rev. **D86**, 035022 (2012), 1205.3499.
[22] R. Dharmapalan et al. (MiniBooNE Collaboration) (2012), 1211.2258.
[23] R. Essig, J. A. Jaros, W. Wester, P. H. Adrian, S. Andreas, et al. (2013), 1311.0029.
[24] *JLab Letter of Intent to PAC (to appear).*
[25] R. Morris and N. Weiner (2011), 1109.3747.
[26] A. C. Vincent, P. Martin, and J. M. Cline, JCAP **1204**, 022 (2012), 1201.0997.
[27] M. Pospelov and A. Ritz, Phys.Lett. **B651**, 208 (2007), hep-ph/0703128.
[28] I. Cholis, L. Goodenough, and N. Weiner, Phys.Rev. **D79**, 123505 (2009), 0802.2922.
[29] B. Batell, M. Pospelov, and A. Ritz, Phys.Rev. **D79**, 115019 (2009), 0903.3396.
[30] M. Battaglieri (2012), URL `http://www.phys.hawaii.edu/~hanohano/post/AAP2012/Battaglieri_Cormorad_AAP12.pdf`.
[31] J. D. Bjorken, R. Essig, P. Schuster, and N. Toro, Phys.Rev. **D80**, 075018 (2009), 0906.0580.
[32] J. Bjorken, S. Ecklund, W. Nelson, A. Abashian, C. Church, et al., Phys.Rev. **D38**, 3375 (1988).
[33] E. Riordan, M. Krasny, K. Lang, P. De Barbaro, A. Bodek, et al., Phys.Rev.Lett. **59**, 755 (1987).
[34] A. Bross, M. Crisler, S. H. Pordes, J. Volk, S. Errede, et al., Phys.Rev.Lett. **67**, 2942 (1991).
[35] R. Essig, P. Schuster, and N. Toro, Phys.Rev. **D80**, 015003 (2009), 0903.3941.
[36] R. Essig, P. Schuster, N. Toro, and B. Wojtsekhowski, JHEP **1102**, 009 (2011), 1001.2557.
[37] B. Batell, M. Pospelov, and A. Ritz, Phys.Rev. **D79**, 115008 (2009), 0903.0363.
[38] P. Fayet, Phys.Rev. **D75**, 115017 (2007), hep-ph/0702176.
[39] M. Freytsis, G. Ovanesyan, and J. Thaler, JHEP **1001**, 111 (2010), 0909.2862.
[40] R. Essig, R. Harnik, J. Kaplan, and N. Toro, Phys.Rev. **D82**, 113008 (2010), 1008.0636.
[41] M. Reece and L.-T. Wang, JHEP **0907**, 051 (2009), 0904.1743.
[42] B. Wojtsekhowski, AIP Conf.Proc. **1160**, 149 (2009), 0906.5265.
[43] G. Amelino-Camelia, F. Archilli, D. Babusci, D. Badoni, G. Bencivenni, et al., Eur.Phys.J. **C68**, 619 (2010), 1003.3868.
[44] M. Baumgart, C. Cheung, J. T. Ruderman, L.-T. Wang, and I. Yavin, JHEP **0904**, 014 (2009), 0901.0283.
[45] H. Merkel et al. (A1 Collaboration), Phys.Rev.Lett. **106**, 251802 (2011), 1101.4091.
[46] T. Beranek, H. Merkel, and M. Vanderhaeghen (2013), 1303.2540.
[47] S. Abrahamyan et al. (APEX Collaboration), Phys.Rev.Lett. **107**, 191804 (2011), 1108.2750.
[48] B. Aubert et al. (BaBar Collaboration), Phys.Rev.Lett. **103**, 081803 (2009), 0905.4539.
[49] B. Echenard, Adv.High Energy Phys. **2012**, 514014 (2012), 1209.1143.
[50] D. Babusci et al. (KLOE-2 Collaboration), Phys.Lett. **B720**, 111 (2013), 1210.3927.
[51] P. Adlarson et al. (WASA-at-COSY Collaboration) (2013), 1304.0671.
[52] M. Davier, J. Jeanjean, and H. Nguyen Ngoc, Phys.Lett. **B180**, 295 (1986).
[53] A. Hook, E. Izaguirre, and J. G. Wacker, Adv.High Energy Phys. **2011**, 859762 (2011), 1006.0973.
[54] D. E. Morrissey and A. P. Spray (2014), 1402.4817.
[55] M. Pospelov, Phys.Rev. **D80**, 095002 (2009), 0811.1030.
[56] B. Aubert et al. (BaBar Collaboration) (2008), 0808.0017.
[57] A. Artamonov et al. (E949 Collaboration), Phys.Rev.Lett. **101**, 191802 (2008), 0808.2459.
[58] G. Bellini, J. Benziger, D. Bick, S. Bonetti, G. Bonfini, et al., Phys.Rev.Lett. **107**, 141302 (2011), 1104.1816.
[59] R. Essig, J. Kaplan, P. Schuster, and N. Toro, Submitted to Physical Review D (2010), 1004.0691.
[60] R. Essig, J. Mardon, M. Papucci, T. Volansky, and Y.-M. Zhong, JHEP **1311**, 167 (2013), 1309.5084.
[61] G. Giudice, P. Paradisi, and M. Passera, JHEP **1211**, 113 (2012), 1208.6583.
[62] P. J. Fox and E. Poppitz, Phys.Rev. **D79**, 083528 (2009), 0811.0399.
[63] M. Cirelli, M. Kadastik, M. Raidal, and A. Strumia, Nucl.Phys. **B813**, 1 (2009), 0809.2409.
[64] C.-R. Chen and F. Takahashi, JCAP **0902**, 004 (2009), 0810.4110.
[65] E. Baltz and L. Bergstrom, Phys.Rev. **D67**, 043516 (2003), hep-ph/0211325.
[66] P. Agrawal, Z. Chacko, and C. B. Verhaaren (2014), 1402.7369.
[67] S. Chang, R. Edezhath, J. Hutchinson, and M. Luty (2014), 1402.7358.
[68] Work to appear (2014).
[69] J. Kremer, M. Boezio, M. Ambriola, G. Barbiellini, S. Bartalucci, et al., Phys.Rev.Lett. **83**, 4241 (1999).
[70] K. J. Kim and Y.-S. Tsai, Phys.Rev. **D8**, 3109 (1973).
[71] R. H. Helm, Phys.Rev. **104**, 1466 (1956).
[72] G. Duda, A. Kemper, and P. Gondolo, JCAP **0704**, 012 (2007), hep-ph/0608035.
[73] B. A. Dobrescu and G. Z. Krnjaic, Phys.Rev. **D85**, 075020 (2012), 1104.2893.